Torque equilibrium spin wave theory of Raman scattering in an anisotropic triangular lattice antiferromagnet with Dzyaloshinskii-Moriya interaction

Chao Shan [1,*] Shangjian Jin [1,*] Trinanjan Datta [2,1,†] and Dao-Xin Yao [1,‡]

[1]*State Key Laboratory of Optoelectronic Materials and Technologies, School of Physics, Sun Yat-Sen University, Guangzhou 510275, China*

[2]*Department of Chemistry and Physics, Augusta University, 1120 15th Street, Augusta, Georgia 30912, USA*

(Received 16 August 2020; revised 29 November 2020; accepted 24 December 2020; published 13 January 2021)

We apply torque equilibrium spin wave theory (TESWT) to investigate an anisotropic XXZ antiferromagnetic model with Dzyaloshinskii-Moriya interaction in a triangular lattice. Considering the quasiparticle vacuum as our reference, we provide an accurate analysis of the noncollinear ground state of a frustrated triangular lattice magnet using the TESWT formalism. We elucidate the effects of quantum fluctuations on the ordering wave vector based on model system parameters. We study the single-magnon dispersion, the two-magnon continuum using the spectral function, and the Raman spectrum of bimagnon and trimagnon excitations. We present our results for the HH, VV, and the HV polarization Raman geometry dependence of the bimagnon and trimagnon excitation spectra where H (V) represents horizontal (vertical) polarization. Our calculations show that both the HH and the HV polarization spectra can be used to determine the degree of anisotropy of our system. We calculate the Raman spectra of $Ba_3CoSb_2O_9$ and Cs_2CuCl_4.

DOI: 10.1103/PhysRevB.103.024417

I. INTRODUCTION

The effect of quantum fluctuations on the ground state and the phase diagram of frustrated magnets has been a topic of interest in recent years [1–8]. The two-dimensional triangular lattice antiferromagnet (TLAF) is a canonical example of a frustrated magnetic system. There are several examples of TLAF (see Table I). Due to the melting of long-range magnetic order by frustration [9,10], the two-dimensional triangular lattice is considered as a natural spin-liquid candidate [11,12]. Even when magnetic long-range order exists, the competition between various interactions has consequences on the ground state and the phase diagram, especially for low-dimensional spin systems [13,14]. Quantum fluctuations can be non-negligible even for ordered magnets with 120° spiral order [15–17].

The noncollinear spin structure of the triangular lattice leads to interesting phenomena such as the presence of a roton minimum [18,19] and a continuum of high-energy magnons [20–22]. Similar to superfluid ^{4}He [23] and fractional quantum Hall systems [24], Zheng *et al.* [20–22] defined the M and M' points of the Brillouin zone (BZ) of a triangular lattice as rotonlike points. The formation of the local minimum is caused by quantum fluctuations [25,26]. The roton signal has been observed in inelastic neutron scattering (INS) experiments [16,18,27,28]. However, the nature of the high-energy continuum in the triangular lattice is still controversial. The continuous excitation at high energy [20–22] may come from fractional excitation of a proximate spin-liquid phase [29–33] or from strong magnon-magnon interactions [34–36]. In this context, Raman spectroscopy serves as a powerful tool to probe lattice distortions and the effect of ground-state quantum fluctuations. It has already been used to detect magnon excitations in TLAF [37–43]. Raman's advantage is the sensitivity to polarization geometry [44] and magnon-magnon interactions [45,46], which is helpful for studying the high-energy continuum. Note, a previous resonant inelastic x-ray scattering (RIXS) calculation [47] on an anisotropic TLAF has investigated the polarization-independent bimagnon and trimagnon spectra.

There are a couple of Raman scattering experiments on the anisotropic triangular lattice compounds α-$CaCr_2O_4$ [40] and α-$SrCr_2O_4$ [41]. However, the model Hamiltonian for these two compounds is complicated. From a theoretical perspective, Raman bimagnon calculation for the TLAF has been performed with a square lattice Raman scattering operator [48] within the framework of interacting spin wave theory [45,46]. However, the presence of divergence in the ordering wave vector and singularity of the spin wave spectrum calls for renewed attention to accurately describe the noncollinear frustrated triangular lattice magnet [47] beyond the $(1/S)$-spin wave theory analysis. The Raman spectrum should be carefully reconsidered with appropriate quantum fluctuation effects and with the proper underlying lattice symmetry. The recently established torque equilibrium spin wave theory (TESWT) considers the spin Casimir effect of a noncollinear system caused by the zero-point quantum fluctuations [13]. This formalism cures the ordering wave vector of any divergence and is as convenient as $(1/S)$-spin wave theory. The computed phase diagram of the anisotropic TLAF is consistent with series expansion (SE) and modified spin wave theory (MSWT) [3,49]. Since quantum fluctuations cause modification of the ordering wave vector, its influence on the magnon

*These authors contributed equally to this work.
†Corresponding author: tdatta@augusta.edu
‡Corresponding author: yaodaox@mail.sysu.edu.cn

 ©2021 American Physical Society

TABLE I. Ordered antiferromagnetic triangular lattice materials. The third (fourth) column is the nearest-neighbor exchange interaction J (ordering wave vector). Our torque equilibrium spin wave theory approach for Raman spectrum calculation can be applied to any of the ordered triangular lattice materials listed below. In this paper, we only report on the Raman scattering spectrum of $Ba_3CoSb_2O_9$ and Cs_2CuCl_4.

Material	Space group	J (meV)	**Q**
$Ba_3CoSb_2O_9$ [50]	$P6_3/mmc$	1.67	(2/3,0,1)
$CuCrO_2$ [51]	$R\bar{3}m$	2.8	(0.658,0,0)
α-$SrCr_2O_4$ [17]	$Pmmn$	$J_{\text{mean}} \approx 5$	(0.6609,0,1)
α-$GaCr_2O_4$ [16]	$Pmmn$	8.8	(0.6659,0,1)
$LuMnO_3$ [22]	$P6_3cm$	9	(2/3,0,0)
Cs_2CuCl_4 [47]	$Pnma$	0.48	(0.530,0,0) [20]
Cs_2CuBr_4 [52]	$Pnma$	1.35	(0.575,0,0)

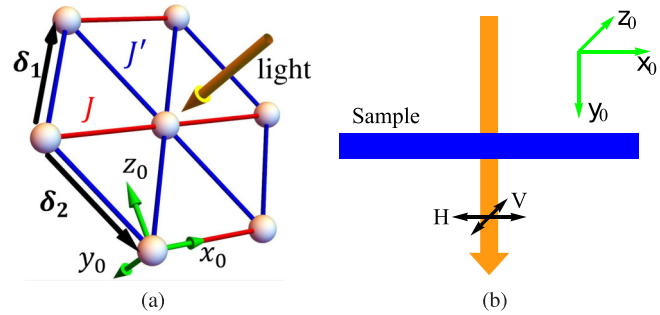

FIG. 1. (a) Triangular lattice with anisotropic exchange constants J and J' acting along the bonds. (b) Experimental geometry setup to study polarization effects within Raman scattering. $\delta_{1,2}$ denotes lattice vectors. H (horizontal) and V (vertical) indicates polarization direction of the incoming and outgoing light.

and multimagnon excitations (bimagnon and trimagnon) is an important question to investigate.

In this study, we extend the analysis of the J-J' triangular lattice Heisenberg magnet to the case of a XXZ model with Dzyaloshinskii-Moriya (DM) interaction. First, we apply TESWT to obtain the ordering wave vector. We find that the DM interaction is more favorable to stabilizing the helix state compared to XXZ anisotropy. Similar to the quasi-one-dimensional helimagnets [14], the mere presence of XXZ anisotropy can lead to a shift in the phase boundary. Second, we calculate the spectral function within the TESWT framework. We find that the magnon excitations are more stable with DM interaction and XXZ anisotropy. Our calculations show the presence of quasiparticle excitation and continuum in the spectral function. Third, we calculate the polarization-dependent bimagnon and trimagnon Raman spectra under TESWT. Distinct from the noninteracting calculation, the bimagnon spectrum in the HV polarization displays a single-peak feature with magnon-magnon interactions considered. We find that the bimagnon intensity is polarization independent for the isotropic TLAF. However, the bimagnon excitation occurs only in HV polarization for the anisotropic TLAF. In the HV polarization, spatial anisotropy reduces the bimagnon intensity and peak energy. DM interaction also reduces its intensity, especially in a system with increasing spatial anisotropy. In spite of a spin gap, DM interaction induces an upshift of the bimagnon peak towards higher energy, while XXZ anisotropy downshifts the bimagnon peak to a slightly lower energy. The trimagon excitation is considerable and contributes to the continuum in the HH polarization for the TLAF. We also compute the Raman spectrum of $Ba_3CoSb_2O_9$ and Cs_2CuCl_4. For $Ba_3CoSb_2O_9$, its Raman spectrum has a sharp peak and a broad shoulder in both the HH and the HV polarizations. For Cs_2CuCl_4, its Raman spectrum has a sharp bimagnon peak in HV polarization. We find that the primary contribution to the Raman intensity in the HH polarization comes from the trimagnon excitation. However, in the HV polarization, both the bimagnon and the trimagnon excitations mix and give a broad spectrum.

This paper is organized as follows. In Sec. II we introduce the XXZ model with spatial anisotropy and DM interaction. In Sec. III we compute the spin wave spectrum and spectral function by applying TESWT. In Sec. IV we utilize TESWT to calculate the bimagnon and trimagnon Raman spectra. In Sec. IV A we derive the expressions for the Raman operator, their polarization dependence, and the magnon-magnon interaction effects. In Sec. IV B we present and discuss our results on spatial anisotropy, spin anisotropy, magnon-magnon interaction, and polarization dependence. Then, we present the Raman spectrum of $Ba_3CoSb_2O_9$ and Cs_2CuCl_4. Finally, in Sec. V we provide our conclusions

II. MODEL

Triangular lattice materials can contain spatial or spin anisotropies. In the case of Cs_2CuCl_4 and Cs_2CuBr_4, DM interaction is present and generates a spin gap. However, the large gap of Cs_2CuBr_4 in the energy dispersion cannot be generated exclusively by the DM interaction [52,53]. Additionally, spin-orbit coupling may lead to XXZ anisotropy which has been used to explain the presence of a gapped spectrum in some TLAF materials [54,55]. Even though $Ba_3CoSb_2O_9$ is spatially isotropic in its exchange interaction, its magnetization is well explained by a spin-$\frac{1}{2}$ XXZ (spin-anisotropic) model on a triangular lattice [50,56–59]. Thus, to conduct a thorough study of the frustrated TLAF systems, we consider XXZ anisotropy in addition to anisotropic exchange interaction and DM interaction. Our model is written as

$$\begin{aligned}\mathcal{H} = J \sum_{\langle ij \rangle}^{\delta_1+\delta_2} \left[S_i^x S_j^x + S_i^z S_j^z + \Delta S_i^y S_j^y\right] \\ + J' \sum_{\langle ij \rangle}^{\delta_1,\delta_2} \left[S_i^x S_j^x + S_i^z S_j^z + \Delta S_i^y S_j^y\right] \\ - \sum_{\langle ij \rangle}^{\delta_1,\delta_2} \mathbf{D} \cdot (\mathbf{S}_i \times \mathbf{S}_j),\end{aligned} \tag{1}$$

where $\langle ij \rangle$ refers to nearest-neighbor bonds on the triangular lattice and $\boldsymbol{\delta}_{1,2}$ are the nearest-neighbor (NN) vectors along the diagonal bonds [see Fig. 1(a)]. The four parameters (J, J', D, Δ) contained in the model correspond to the exchange constants along the horizontal bonds, the exchange constants along the diagonal bonds, DM interaction along

the y_0 direction ($D > 0$) [20], and XXZ spin anisotropy, respectively.

The spin spiral ground state can be described by an ordering wave vector $\mathbf{Q}$. To analyze the spin wave spectrum of this magnetic model, we first transform from the laboratory to the rotated local coordinate frame [47]. Then, successive applications of the Holstein-Primakoff (HP), the Fourier, and the Bogoliubov transformations give us the effective first-order $1/S$ expansion Hamiltonian as

$$\begin{aligned}\mathcal{H}_{\text{eff}} = &\sum_{\mathbf{k}}\left[(S\varepsilon_{\mathbf{k}}+\delta\varepsilon_{\mathbf{k}})c^{\dagger}_{\mathbf{k}}c_{\mathbf{k}}+\frac{O_{\mathbf{k}}}{2}(c^{\dagger}_{\mathbf{k}}c^{\dagger}_{-\mathbf{k}}+c_{\mathbf{k}}c_{-\mathbf{k}})\right]\\ &+\left\{i\sqrt{\frac{S}{2N}}\left[\frac{1}{2!}\sum_{\{\mathbf{k}_i\}}\Phi_a(1,2;3)c^{\dagger}_1c^{\dagger}_2c_3\right.\right.\\ &\left.\left.+\frac{1}{3!}\sum_{\{\mathbf{k}_i\}}\Phi_b(1,2,3)c^{\dagger}_1c^{\dagger}_2c^{\dagger}_3\right]+\text{H.c.}\right\}\\ &+\frac{1}{8N}\sum_{\{\mathbf{k}_i\}}\Phi_c(1,2;3,4)c^{\dagger}_1c^{\dagger}_2c_3c_4, \qquad (2)\end{aligned}$$

where $c^{\dagger}_{\mathbf{k}}$ ($c_{\mathbf{k}}$) is the quasiparticle creation (annihilation) operator in momentum space. The numbers 1, 2, 3, ...denote the wave vectors $\mathbf{k}_1, \mathbf{k}_2, \mathbf{k}_3, \ldots$. The formulas of the vertex coefficients Φ_a, Φ_b, and Φ_c are given in the Appendix. We set $J = 1$ meV in all our subsequent calculations. Thus, our model has three parameters (J', D, Δ), where J' and D represent interaction strength relative to the exchange interaction J. In the next section, we will analyze the above bosonized Hamiltonian for its spin wave spectrum. As mentioned before, the $(1/S)$-spin wave theory cannot treat the quantum fluctuations appropriately, which in turn leads to divergences and singularities in the calculation of the ground state [14]. Thus, we will analyze this model using TESWT.

III. TESWT SPIN WAVE SPECTRUM

Torque equilibrium spin wave theory formalism gives the correct ground state and phase diagram for spin spiral magnets [13,14,47]. The phase diagram that results from TESWT formalism is consistent with previous numerical calculations [3,49]. The essential conceptual difference between spin wave theory and TESWT is the reference ground state. The former considers the classical vacuum as the ground state, while the later considers the quasiparticle vacuum state as the correct starting point. Although linear spin wave spectrum $\varepsilon_{\mathbf{k}}$ is physically well behaved at the classical ordering wave vector $\mathbf{Q}_{cl} = (Q_{cl}, 0, 0)$, it yields an incorrect ground-state wave vector (see Fig. 2). Within the TESWT approach the goal is to find a redefined Hamiltonian whose classical ordering wave vector $\widetilde{\mathbf{Q}}_{cl}$ is equal to the final ordering wave vector $\mathbf{Q}$ of the original state. Henceforth, the tilde variable will signify parameters of the torque equilibrium shifted Hamiltonian.

To implement TESWT we rewrite the quadratic term of our model as $H_2(J', D, \Delta, \mathbf{Q}) = \widetilde{H}_2(\widetilde{J}', \widetilde{D}, \widetilde{\Delta}, \mathbf{Q}) + H^c_2$, where the superscript c represents the counterterm which will regularize the original singular Hamiltonian. Due to the small values of D and $(1-\Delta)$ in real materials, we take $\widetilde{D} = D$ and $\widetilde{\Delta} = \Delta$.

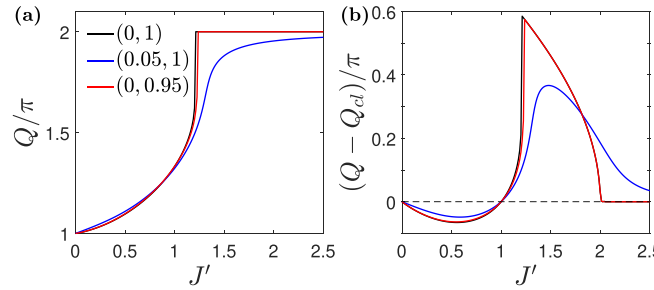

FIG. 2. Ordering wave vector (a) Q/π and (b) $(Q - Q_{cl})/\pi$ versus J' for spin-$\frac{1}{2}$ system. The black, blue, and red lines show results for parameters (D, Δ) equal to (0,1), (0.05,1), and (0,0.95), respectively.

Next, the spin Casimir torque is defined as

$$\mathbf{T}_{sc}(\mathbf{Q}) = \sum_{\mathbf{k}}\left\langle\Psi_{\text{vac}}\left|\frac{\partial H_{sw}}{\partial\mathbf{Q}}\right|\Psi_{\text{vac}}\right\rangle, \qquad (3)$$

where $|\Psi_{\text{vac}}\rangle$ represents the expectation value of the quasiparticle vacuum state. Next, we utilize the torque equilibrium condition, within the approximation of $\mathbf{T}_{sc}(\mathbf{Q}) = \widetilde{\mathbf{T}}_{sc}(\mathbf{Q})$, to obtain the final ordering wave vector as

$$\frac{\partial E_0(\mathbf{Q})}{\partial\mathbf{Q}} + \frac{S}{2}\sum_{\mathbf{k}}\frac{\partial\widetilde{\varepsilon}_{\mathbf{k}}}{\partial\mathbf{Q}} = 0, \qquad (4)$$

where $\widetilde{F} = F(\widetilde{J}', \widetilde{D}, \widetilde{\Delta}, \mathbf{Q})$ (F is an arbitrary operator here). The corresponding functions are shown in the Appendix.

Figure 2(a) shows the ordering vector Q of the spin-$\frac{1}{2}$ system obtained using TESWT. Without DM interaction and XXZ anisotropy, the TLAF orders in an antiferromagnet phase for $J' \geqslant 1.2$. DM interaction influences the ordering wave vector more than XXZ anisotropy. It enlarges the region of spiral phase. Figure 2(b) shows the difference of ordering vector between TESWT and linear spin wave theory (LSWT). For $J' \leqslant 1$, TESWT gives a smaller Q (compared to LSWT) and the ground state becomes closer to the ferromagnet. Whereas, with $J' \geqslant 1$ TESWT gives a larger Q and the ground state will be nearly antiferromagnetic in arrangement. Thus, we conclude that the spin Casimir effect induces collinear arrangement of spins. Since we are analyzing a coplanar noncollinear spin configuration we will restrict our XXZ anisotropy values. It is evident from Fig. 2(b) that with DM interaction, the difference between TESWT and LSWT becomes smaller, indicating that it weakens quantum fluctuations. The Hamiltonian shift results in the one-loop torque equilibrium effective Hamiltonian given by

$$\begin{aligned}\widetilde{\mathcal{H}}_{\text{eff}} = &\sum_{\mathbf{k}}\left[(S\widetilde{\varepsilon}_{\mathbf{k}}+\delta\widetilde{\varepsilon}_{\mathbf{k}})c^{\dagger}_{\mathbf{k}}c_{\mathbf{k}}+\frac{\widetilde{O}_{\mathbf{k}}}{2}(c^{\dagger}_{\mathbf{k}}c^{\dagger}_{-\mathbf{k}}+c_{\mathbf{k}}c_{-\mathbf{k}})\right.\\ &\left.+S\varepsilon^{c}_{\mathbf{k}}c^{\dagger}_{\mathbf{k}}c_{\mathbf{k}}+\frac{SO^{c}_{\mathbf{k}}}{2}(c^{\dagger}_{\mathbf{k}}c^{\dagger}_{-\mathbf{k}}+c_{\mathbf{k}}c_{-\mathbf{k}})\right]\\ &+\left\{i\sqrt{\frac{S}{2N}}\left[\frac{1}{2!}\sum_{\{\mathbf{k}_i\}}\widetilde{\Phi}_a(1,2;3)c^{\dagger}_1c^{\dagger}_2c_3\right.\right.\end{aligned}$$

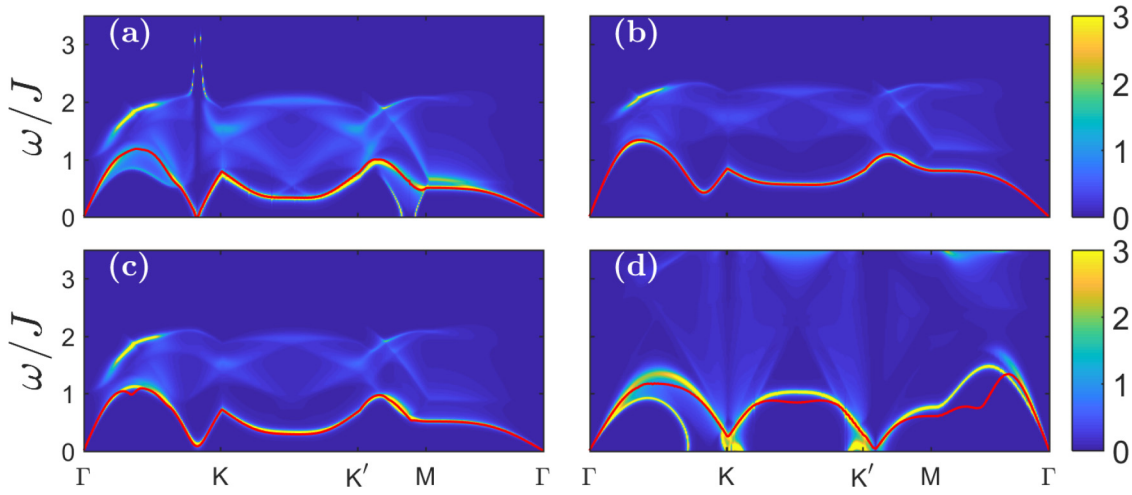

FIG. 3. Momentum and energy dependence of the spectral function $A(\mathbf{k}, \omega)$ for a spin-$\frac{1}{2}$ system. The points in the chosen path are defined as $\Gamma = (0, 0)$, $K = (4\pi/3, 0)$, $K' = (2\pi/3, 2\pi/\sqrt{3})$, and $M = (0, 2\pi/\sqrt{3})$. The parameters (J', D, Δ) are (a) (0.5,0,1), (b) (0.5,0.05,1), (c) (0.5,0,0.95), and (d) (1.1,0,1). The solid red lines show the on-shell dispersion $\omega_{\mathbf{k}}$ [see Eq. (9)].

$$+\frac{1}{3!}\sum_{\{\mathbf{k}_i\}}\widetilde{\Phi}_b(1,2,3)c_1^\dagger c_2^\dagger c_3^\dagger\Big]+\text{H.c.}\Big\}$$
$$+\frac{1}{8N}\sum_{\{\mathbf{k}_i\}}\widetilde{\Phi}_c(1,2;3,4)c_1^\dagger c_2^\dagger c_3 c_4, \tag{5}$$

with

$$\varepsilon_{\mathbf{k}}^c=\frac{1}{\widetilde{\varepsilon}_{\mathbf{k}}}(\widetilde{A}_{\mathbf{k}}A_{\mathbf{k}}-\widetilde{B}_{\mathbf{k}}B_{\mathbf{k}})-\widetilde{\varepsilon}_{\mathbf{k}},$$
$$O_{\mathbf{k}}^c=\frac{1}{\widetilde{\varepsilon}_{\mathbf{k}}}(\widetilde{A}_{\mathbf{k}}B_{\mathbf{k}}-\widetilde{B}_{\mathbf{k}}A_{\mathbf{k}}). \tag{6}$$

In such a noncollinear spin system, we consider the renormalization of magnon dispersion up to $1/S$ order. Thus, the counterterm contributions from H_3 and H_4 are neglected [13,14]. Within this scheme the first-order renormalized Green's function in the one-loop approximation is given by

$$G^{-1}(\mathbf{k},\omega)=\omega-S\widetilde{\varepsilon}_{\mathbf{k}}-\big[S\varepsilon_{\mathbf{k}}^c$$
$$+\widetilde{\Sigma}_c(\mathbf{k})+\widetilde{\Sigma}_3^a(\mathbf{k},\omega)+\widetilde{\Sigma}_3^b(\mathbf{k},\omega)\big], \tag{7}$$

where $S\varepsilon_{\mathbf{k}}^c$ is the counterterm from H_2. $\widetilde{\Sigma}_c(\mathbf{k})=\delta\widetilde{\varepsilon}_{\mathbf{k}}$ describes the quartic correction following mean-field averages. $\widetilde{\Sigma}_3^{a,b}(\mathbf{k},\omega)$ are the self-energy contributions from the cubic interaction and are given by

$$\widetilde{\Sigma}_3^a(\mathbf{k},\omega)=\frac{S}{4N}\sum_{\mathbf{k}_1}\frac{|\widetilde{\Phi}_a(\mathbf{k}_1,\mathbf{k}-\mathbf{k}_1;\mathbf{k})|^2}{\omega-S\widetilde{\varepsilon}_{\mathbf{k}_1}-S\widetilde{\varepsilon}_{\mathbf{k}-\mathbf{k}_1}+i0^+},$$
$$\widetilde{\Sigma}_3^b(\mathbf{k},\omega)=-\frac{S}{4N}\sum_{\mathbf{k}_1}\frac{|\widetilde{\Phi}_b(\mathbf{k}_1,-\mathbf{k}-\mathbf{k}_1,\mathbf{k})|^2}{\omega+S\widetilde{\varepsilon}_{\mathbf{k}_1}+S\widetilde{\varepsilon}_{\mathbf{k}+\mathbf{k}_1}-i0^+}. \tag{8}$$

The on-shell approximation for the renormalized Green's function, in the self-energy contribution, is given by $\omega_{\mathbf{k}} = S\widetilde{\varepsilon}_{\mathbf{k}}$. Thus, the first-order renormalized magnon energy can be calculated as

$$\omega_{\mathbf{k}}=S\widetilde{\varepsilon}_{\mathbf{k}}+S\varepsilon_{\mathbf{k}}^c+\widetilde{\Sigma}_c(\mathbf{k})+\widetilde{\Sigma}_3^a(\mathbf{k},S\widetilde{\varepsilon}_{\mathbf{k}})+\widetilde{\Sigma}_3^b(\mathbf{k},S\widetilde{\varepsilon}_{\mathbf{k}}). \tag{9}$$

Note, all our derivations are applicable for both low- and high-spin values. Quantum fluctuations are maximal when $S = \frac{1}{2}$, as is in our case. The real and imaginary parts of $\omega_{\mathbf{k}}$ are the magnon dispersion and the magnon decay, respectively. To obtain an intuitive understanding of the single-magnon excitation, we calculate the spectral function, which is defined as

$$A(\mathbf{k},\omega)=-\frac{1}{\pi}\text{Im}G(\mathbf{k},\omega). \tag{10}$$

In Fig. 3 we report our spectral function calculation for various model parameters. The intensity plots show broadening of the quasiparticle excitation and presence of two-magnon continuum in all the panels, which is consistent with a previous study on the isotropic TLAF [36]. Thus, magnon-magnon interactions are important in the triangular lattice. Compared to Ref. [36], spatial anisotropy causes a downshift of the continuum energy. In Fig. 3(a) the dispersion shows no gap at the ordering wave vector. This is consistent because the DM interaction is set to zero and the Hamiltonian is at the spin-isotropic point $\Delta = 1$. From Figs. 3(b) and 3(c) we observe that DM interaction and XXZ anisotropy can suppress damping and stabilize magnon excitations. Both XXZ anisotropy and DM interaction can generate gaps at the ordering wave vector, thereby reducing magnon decay. However, DM interaction has a greater effect of suppression on magnon decay than XXZ anisotropy. In Fig. 3(b), the consistency between the spectral function and dispersion indicates that the on-shell calculation is more reasonable with DM interaction. However, the spectrum is inconsistent with the on-shell dispersion when $J' > 1$ [see Fig. 3(d)]. Thus, we restrict our Raman calculations to parameters where the spatially anisotropic exchange interaction does not exceed one. In fact, this is a valid parameter regime for real materials [47,50,52,54].

IV. TORQUE EQUILIBRIUM SPIN WAVE THEORY RAMAN SPECTRUM

Raman scattering has the ability to detect magnon excitations due to its sensitivity to magnon-magnon interactions

and polarization [37–41,44–46,60]. Thus, we consider interactions to study the continuum shown in Fig. 3. Experimental data from INS indicate that the highest energy of a single magnon is about 20 meV [17]. Considering the presence of magnetic interactions in a real material (which are known to introduce downshifts in the Raman spectrum), it is debatable whether the high-energy excitation above 40 meV in the unpolarized Raman experiment [41] of α-$SrCr_2O_4$ may be attributed to a bimagnon. Based on our calculations and the location of the Raman spectrum peaks, we conclude that it most probably contains the trimagnon excitation. Thus, the study of trimagnon Raman spectrum is valuable. In addition to the unpolarized Raman detection, a polarization-dependent Raman spectrum will provide further perspective on the understanding of bimagnon and trimagnon excitation. Hence, we study polarized Raman scattering of TLAF to investigate the bimagnon and trimagnon excitation behaviors. In comparison to RIXS, Raman scattering is a more mature technique restricted to scattering momentum $\mathbf{q} \approx 0$. For the bimagnon, the momentum of individual magnons can be nonzero, as long as the momenta of the two magnons approximately sum to zero. The same rule applies to the trimagnon.

To date, from a theoretical perspective, a substantial number of studies have been pursued within LSWT and an interacting framework to investigate the Raman spectrum of TLAF Heisenberg model [37,38,45,46]. However, since LSWT leads to a divergent ordering wave vector and fails to describe the ground state, it is not suitable to calculate the magnon excitation. Thus, we apply the TESWT to study the Raman bimagnon and trimagnon excitations of TLAF. One of the key developments reported in this paper is on trimagnon calculation and our discussion of the polarization dependence of the bimagnon and trimagnon excitations. Neglecting polarization, the bimagnon intensity is zero at the Γ point. However, the real spectrum of the anisotropic TLAF is polarization dependent. Next, we discuss the polarization dependence and how it helps to analyze the composition of Raman spectrum.

A. Raman scattering operator and interactions

Standard perturbation theory formalism applied to electron-radiation interaction can be used to compute the Raman scattering cross section [61–63]. Since we are studying magnetic Raman scattering, the operator should be expressed in terms of spin operators which obey the underlying lattice symmetry. Our triangular lattice model Hamiltonian contains spatial anisotropy, DM interaction, and XXZ anisotropy. Thus, the expression for the polarization-dependent second-order Raman scattering operator is

$$\hat{\mathcal{O}} = \sum_{i,\pm\boldsymbol{\delta}_j} \mathcal{P}_j(\theta,\phi)\big[J_j\big(S_i^x S_{i+\boldsymbol{\delta}_j}^x + S_i^z S_{i+\boldsymbol{\delta}_j}^z + \Delta S_i^y S_{i+\boldsymbol{\delta}_j}^y\big) - \mathbf{D}_j \cdot \big(\mathbf{S}_i \times \mathbf{S}_{i+\boldsymbol{\delta}_j}\big)\big], \tag{11}$$

where $\boldsymbol{\delta}_j$ denote the lattice vectors: $\boldsymbol{\delta}_1 = (\frac{1}{2}, 0, \frac{\sqrt{3}}{2})$, $\boldsymbol{\delta}_2 = (\frac{1}{2}, 0, -\frac{\sqrt{3}}{2})$, and $\boldsymbol{\delta}_3 = (1, 0, 0)$.[1] The polarization geometry and the symmetry of the experimental setup are captured in the $\mathcal{P}_j(\theta,\phi)$ operator coefficient. We consider the polarization of the incoming and outgoing light as $\hat{\boldsymbol{\varepsilon}}_{\text{in}} = (\cos\theta, 0, \sin\theta)$ and $\hat{\boldsymbol{\varepsilon}}_{\text{out}} = (\cos\phi, 0, \sin\phi)$, respectively, where θ and ϕ are defined with respect to the x_0 axis. The sketch of the experimental geometry is shown in Fig. 1(b). Lattice symmetry was employed to analyze the different types of magnetic excitations. Since we are considering a quasi-2D TLAF, for generality, we calculated the Raman spectrum of both the isotropic (C_{3v}) and the anisotropic case (C_{2v}), respectively. The Raman-active modes of the C_{3v} and C_{2v} systems are given by the irreducible representations $A_1 + E$ and $A_1 + A_2$, respectively.

In terms of the Bogoliubov magnons the polarized Raman scattering operator takes the following form:

$$\hat{\mathcal{O}} = \sum_{\mathbf{k}} \widetilde{\mathcal{B}}_{\mathbf{k}}(c_{\mathbf{k}} c_{-\mathbf{k}} + c_{\mathbf{k}}^\dagger c_{-\mathbf{k}}^\dagger) + \sum_{\mathbf{k},\mathbf{p}} \widetilde{\mathcal{F}}(\mathbf{p}, -\mathbf{k}-\mathbf{p}, \mathbf{k})(c_{\mathbf{p}} c_{-\mathbf{k}-\mathbf{p}} c_{\mathbf{k}} - c_{\mathbf{p}}^\dagger c_{-\mathbf{k}-\mathbf{p}}^\dagger c_{\mathbf{k}}^\dagger), \tag{12}$$

where the scattering matrix element $\widetilde{\mathcal{B}}_{\mathbf{k}}$ and $\widetilde{\mathcal{F}}(\mathbf{k}, -\mathbf{k}-\mathbf{p}, \mathbf{p})$ are given by

$$\widetilde{\mathcal{B}}_{\mathbf{k}} = S\sum_{j=1}^{3} \mathcal{P}_j(\theta,\phi)\big[\widetilde{\mu}_{\mathbf{k}}\widetilde{v}_{\mathbf{k}}\xi_{j\mathbf{k}} - \big(\widetilde{\mu}_{\mathbf{k}}^2 + \widetilde{v}_{\mathbf{k}}^2\big)\lambda_{j\mathbf{k}}\big] \tag{13}$$

and

$$\begin{aligned}\widetilde{\mathcal{F}}(\mathbf{k}, -\mathbf{k}-\mathbf{p}, \mathbf{p}) &= \frac{i\sqrt{2S}}{3}\sum_{j=1}^{3}\mathcal{P}_j(\theta,\phi) \\ &\times [\zeta_{j\mathbf{p}}(\widetilde{\mu}_{\mathbf{p}} + \widetilde{v}_{\mathbf{p}}) \times (\widetilde{\mu}_{-\mathbf{k}-\mathbf{p}}\widetilde{v}_{\mathbf{k}} + \widetilde{v}_{-\mathbf{k}-\mathbf{p}}\widetilde{\mu}_{\mathbf{k}}) \\ &+ \zeta_{j,-\mathbf{k}-\mathbf{p}}(\widetilde{\mu}_{-\mathbf{k}-\mathbf{p}} + \widetilde{v}_{-\mathbf{k}-\mathbf{p}}) \times (\widetilde{\mu}_{\mathbf{k}}\widetilde{v}_{\mathbf{p}} + \widetilde{v}_{\mathbf{k}}\widetilde{\mu}_{\mathbf{p}}) \\ &+ \zeta_{j\mathbf{k}}(\widetilde{\mu}_{\mathbf{k}} + \widetilde{v}_{\mathbf{k}}) \times (\widetilde{\mu}_{\mathbf{p}}\widetilde{v}_{-\mathbf{k}-\mathbf{p}} + \widetilde{v}_{\mathbf{p}}\widetilde{\mu}_{-\mathbf{k}-\mathbf{p}})].\end{aligned} \tag{14}$$

We note that the summation of the momenta in the bimagnon (trimagnon) scattering matrix element adds up to zero. In the above equations we have introduced the following functions:

$$\begin{aligned}\xi_{j\mathbf{k}} &= 2[\Delta J_j + J_j\cos(\mathbf{Q}\cdot\boldsymbol{\delta}_j) - D_j\sin(\mathbf{Q}\cdot\boldsymbol{\delta}_j)]\cos(\mathbf{k}\cdot\boldsymbol{\delta}_j) \\ &\quad - 4[J_j\cos(\mathbf{Q}\cdot\delta_j) - D_j\sin(\mathbf{Q}\cdot\boldsymbol{\delta}_j)], \\ \lambda_{j\mathbf{k}} &= [\Delta J_j - J_j\cos(\mathbf{Q}\cdot\boldsymbol{\delta}_j) + D_j\sin(\mathbf{Q}\cdot\boldsymbol{\delta}_j)]\cos(\mathbf{k}\cdot\boldsymbol{\delta}_j), \\ \zeta_{j\mathbf{k}} &= -[J_j\sin(\mathbf{Q}\cdot\boldsymbol{\delta}_j) + D_j\cos(\mathbf{Q}\cdot\boldsymbol{\delta}_j)]\sin(\mathbf{k}\cdot\boldsymbol{\delta}_j).\end{aligned} \tag{15}$$

[1]Note, in our earlier publication (Jin *et al.* [47]), there was a typographical error in the reported RIXS scattering operator expression. The expression missed the DM interaction term which was considered in our study. The correct reported form of the RIXS operator expression should be $\mathcal{R}_{\mathbf{q}} = \sum_{i,\delta} e^{i\mathbf{q}\cdot\mathbf{r}_i}[J_{i\delta}\mathbf{S}_i \cdot \mathbf{S}_{i+\delta} - \mathbf{D}_\delta \cdot (\mathbf{S}_i \times \mathbf{S}_{i+\delta})]$.

For the C_{3v} symmetry the $\mathcal{P}_j(\theta,\phi)$ coefficient is given by the following function:

$$\mathcal{P}_j(\theta,\phi) = \varepsilon_{\rm in}(\theta)\begin{pmatrix} p_1 & & \\ & p_2 & \\ & & p_1 \end{pmatrix}\varepsilon^{\rm T}_{\rm out}(\phi)\alpha_j^{A_1} + \varepsilon_{\rm in}(\theta)\begin{pmatrix} p_3 & & \\ & p_4 & \\ & p_4 & -p_3 \end{pmatrix}\varepsilon^{\rm T}_{\rm out}(\phi)\alpha_j^{E_1} + \varepsilon_{\rm in}(\theta)\begin{pmatrix} & -p_4 & -p_3 \\ -p_4 & & \\ -p_3 & & \end{pmatrix}\varepsilon^{\rm T}_{\rm out}(\phi)\alpha_j^{E_2}, \quad (16)$$

with $\alpha_j^{A_1}=1$, $\alpha_3^{E_1}=-2\alpha_1^{E_1}=-2\alpha_2^{E_1}=1/2$, $\alpha_3^{E_2}=0$, and $\alpha_1^{E_2}=-\alpha_2^{E_2}=\sqrt{3}/4$ [37,38]. We note that each irreducible representation contains an overall multiplicative form factor exclusive to that channel. Within the polarization defined above, the scattering spectrum is dependent only on the (p_1, p_3) coefficients. To proceed with the calculation (in the absence of adequate information to calculate these form factors) we make a simplification by setting $p_1 = p_3 = 1$ in all subsequent calculations. Note, $\varepsilon^{\rm T}_{\rm out}$ is the transpose of $\varepsilon_{\rm out}$. For the C_{2v} symmetry, the $\mathcal{P}_j(\theta,\phi)$ coefficient is given by

$$\mathcal{P}_j(\theta,\phi) = \varepsilon_{\rm in}(\theta)\begin{pmatrix} p_5 & & \\ & p_6 & \\ & & p_7 \end{pmatrix}\varepsilon^{\rm T}_{\rm out}(\phi)\eta_j^{A_1} + \varepsilon_{\rm in}(\theta)\begin{pmatrix} & & p_8 \\ & 0 & \\ p_8 & & \end{pmatrix}\varepsilon^{\rm T}_{\rm out}(\phi)\eta_j^{A_2}, \quad (17)$$

with $\eta_j^{A_1}=1$, $\eta_3^{A_2}=0$, and $\eta_1^{A_2}=-\eta_2^{A_2}=\sqrt{3}/4$. Within the defined polarization, the spectrum is independent of the p_6 coefficient. To simplify, we set $p_5 = p_7 = p_8 = 1$ in our computations.

According to the fluctuation-dissipation theorem, the Raman scattering intensity can be related to the multimagnon susceptibility. In our particular case, the bimagnon and trimagnon susceptibilities are defined as

$$\chi_2(\omega) = \int_0^\beta d\tau\, e^{iw\tau}\sum_{\mathbf{k}\mathbf{k}'}\widetilde{\mathcal{B}}_{\mathbf{k}}\widetilde{\mathcal{B}}_{\mathbf{k}'}\langle T_\tau c_{\mathbf{k}}(\tau)c_{-\mathbf{k}}(\tau)c^\dagger_{\mathbf{k}'}c^\dagger_{-\mathbf{k}'}\rangle, \quad (18)$$

$$\chi_3(\omega) = \int_0^\beta d\tau\, e^{iw\tau}\sum_{\mathbf{k}\mathbf{k}'\mathbf{p}\mathbf{p}'}\widetilde{\mathcal{F}}_{\mathbf{k},\mathbf{p}}\widetilde{\mathcal{F}}_{\mathbf{k}',\mathbf{p}'} \times \langle T_\tau c_{\mathbf{k}}(\tau)c_{-\mathbf{k}-\mathbf{p}}(\tau)c_{\mathbf{p}}(\tau)c^\dagger_{\mathbf{k}'}c^\dagger_{-\mathbf{k}'-\mathbf{p}'}c^\dagger_{\mathbf{p}'}\rangle, \quad (19)$$

where T_τ is the time-ordering operator. $\langle\cdot\rangle$ is the average of the ground state. Here, we study the case of zero temperature $\beta = 1/k_BT$. According to Fermi's golden rule, the noninteracting scattering intensity is related to the bare Green's function $\mathrm{G}_0(\mathbf{k},\omega) = 1/(\omega-\omega^{(0)}_{\mathbf{k}}+i0^+)$ with $\omega^{(0)}_{\mathbf{k}} = S\widetilde{\varepsilon}_{\mathbf{k}}$ in the quasiparticle representation. Applying Wick's theorem, the noninteracting spectrum can be calculated as

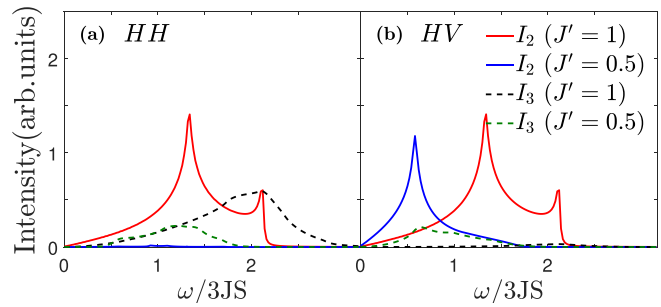

FIG. 4. Noninteracting bimagnon (solid lines) and trimagnon (dashed lines) Raman spectra of spin-$\frac{1}{2}$ system in (a) HH and (b) HV polarizations. DM interaction and XXZ anisotropy are absent in the system. The red and black lines are calculated with $J'=1$ under C_{3v} symmetry. The blue and green lines are calculated with $J'=0.5$ under C_{2v} symmetry.

$$I_2(\omega) = 2\sum_{\mathbf{k}}\widetilde{\mathcal{B}}^2_{\mathbf{k}}\delta\big(\omega-\omega^{(0)}_{\mathbf{k}}-\omega^{(0)}_{\mathbf{k}}\big),$$
$$I_3(\omega) = 6\sum_{\mathbf{k},\mathbf{p}}\widetilde{\mathcal{F}}^2_{\mathbf{k},-\mathbf{k}-\mathbf{p},\mathbf{p}}\delta\big(\omega-\omega^{(0)}_{\mathbf{k}}-\omega^{(0)}_{-\mathbf{k}-\mathbf{p}}-\omega^{(0)}_{\mathbf{p}}\big). \quad (20)$$

The noninteracting result is shown in Fig. 4 and will be discussed in Sec. IV B along with the interacting case.

Next, we consider the $1/S$ correction to the bimagnon excitation. The two-particle propagator $\Pi_{\mathbf{k}\mathbf{k}'}(\omega)$ from Eq. (18) is given by

$$\Pi_{\mathbf{k}\mathbf{k}'}(\omega) = 2i\int\frac{d\omega'}{2\pi}\mathrm{G}_{\mathbf{k}}(\omega+\omega')\mathrm{G}_{-\mathbf{k}}(-\omega')\Gamma_{\mathbf{k}\mathbf{k}'}(\omega,\omega'). \quad (21)$$

The vertex function $\Gamma_{\mathbf{k}\mathbf{k}'}(\omega,\omega')$ can be computed from the Bethe-Salpeter equation which is expressed as [64]

$$\Gamma_{\mathbf{k}\mathbf{k}'}(\omega,\omega') = \delta_{\mathbf{k}\mathbf{k}'} + \sum_{\mathbf{k}_1}2i\int\frac{d\omega_1}{2\pi}\mathrm{G}_{\mathbf{k}_1}(\omega+\omega_1)\mathrm{G}_{-\mathbf{k}_1}(-\omega_1) \times \mathcal{V}^{\rm IR}_{\mathbf{k}\mathbf{k}_1}(\omega',\omega_1)\Gamma_{\mathbf{k}_1\mathbf{k}'}(\omega,\omega_1), \quad (22)$$

where $\mathcal{V}^{\rm IR}_{\mathbf{k}\mathbf{k}_1}(\omega',\omega_1) = \mathcal{V}^3_{\mathbf{k}\mathbf{k}_1}(\omega',\omega_1) + \mathcal{V}^4_{\mathbf{k}\mathbf{k}_1}$ is the two-particle irreducible vertex. For the Raman process, the scattering momentum $\mathbf{q}\approx 0$, thus leading to the disappearance of vertices $\mathcal{V}^{(c)}_3$ and $\mathcal{V}^{(d)}_3$. Thus, the cubic vertex is calculated as

$$\mathcal{V}^3_{\mathbf{k}\mathbf{k}_1}(\omega',\omega_1) = \frac{S}{(8N)}[\widetilde{\Phi}_a(\mathbf{k}_1,\mathbf{k}-\mathbf{k}_1;\mathbf{k})\widetilde{\Phi}^*_a(-\mathbf{k},\mathbf{k}-\mathbf{k}_1;-\mathbf{k}_1) \times \mathrm{G}_0(\mathbf{k}-\mathbf{k}_1,\omega'-\omega_1) + \widetilde{\Phi}^*_a(\mathbf{k},\mathbf{k}_1-\mathbf{k};\mathbf{k}_1)\widetilde{\Phi}_a(-\mathbf{k}_1,\mathbf{k}_1-\mathbf{k};-\mathbf{k}) \times \mathrm{G}_0(\mathbf{k}_1-\mathbf{k},\omega_1-\omega')]. \quad (23)$$

The four-point vertex $\mathcal{V}^4_{\mathbf{k}\mathbf{k}_1}$ originating from the quartic Hamiltonian is given for our Raman case as

$$\begin{aligned}\mathcal{V}^4_{\mathbf{k}\mathbf{k}_1} = \frac{1}{4N}\Big[4\Big(A_0 + B_0 + \frac{1}{2}A_{\mathbf{k}+\mathbf{k}_1} + \frac{1}{2}B_{\mathbf{k}+\mathbf{k}_1} + \frac{1}{2}A_{\mathbf{k}-\mathbf{k}_1} \\ + \frac{1}{2}B_{\mathbf{k}-\mathbf{k}_1} - A_{\mathbf{k}} - A_{\mathbf{k}_1}\Big)\mu_{\mathbf{k}}\mu_{\mathbf{k}1}\upsilon_{\mathbf{k}}\upsilon_{\mathbf{k}1} \\ + (A_{\mathbf{k}-\mathbf{k}_1} + B_{\mathbf{k}-\mathbf{k}_1} + A_{\mathbf{k}+\mathbf{k}_1} + B_{\mathbf{k}+\mathbf{k}_1} - A_{\mathbf{k}} - A_{\mathbf{k}_1}) \\ \times \big(\mu^2_{\mathbf{k}}\mu^2_{\mathbf{k}_1} + \upsilon^2_{\mathbf{k}}\upsilon^2_{\mathbf{k}_1}\big) - (2B_{\mathbf{k}} + B_{\mathbf{k}_1})\big(\mu^2_{\mathbf{k}} + \upsilon^2_{\mathbf{k}}\big)\mu_{\mathbf{k}_1}\upsilon_{\mathbf{k}_1} \\ - (2B_{\mathbf{k}_1} + B_{\mathbf{k}})\big(\mu^2_{\mathbf{k}_1} + \upsilon^2_{\mathbf{k}_1}\big)\mu_{\mathbf{k}}\upsilon_{\mathbf{k}}\Big]. \qquad (24)\end{aligned}$$

Next, considering the appropriate time domain of $\tau \in [-\infty, \infty]$, the expression for the interacting bimagnon Raman intensity is given by

$$I_2(\omega) = -\frac{1}{\pi}\mathrm{Im}\sum_{\mathrm{m,n}}[\hat{\chi}_{\mathrm{mn}}(\omega) - \hat{\chi}_{\mathrm{mn}}(-\omega)]. \qquad (25)$$

In the above calculation we will assume that the two on-shell magnons are created and annihilated in the intermediate propagators with $\omega' \approx -\omega^{(0)}_{\mathbf{k}} = -S\widetilde{\varepsilon}_{\mathbf{k}} - S\varepsilon^c_{\mathbf{k}}$ and $\omega_1 \approx -\omega^{(0)}_{\mathbf{k}_1} = -S\widetilde{\varepsilon}_{\mathbf{k}_1} - S\varepsilon^c_{\mathbf{k}_1}$. We calculate the bimagnon susceptibility in the matrix form $\hat{\chi}^T = \widetilde{\mathcal{B}}_{\mathbf{k}}[\hat{\mathbf{1}} - \hat{\Gamma}_{\mathbf{k},\mathbf{p}}]^{-1}\Pi_{\mathbf{k}}\widetilde{\mathcal{B}}_{\mathbf{k}}$, where $\Pi_{\mathbf{k}} = 2[\omega - 2\omega_{\mathbf{k}} + i0^+]^{-1}$ is the renormalized two-magnon propagator [47,64].

B. Bimagnon and trimagnon Raman spectra

We calculate the spectrum under HH, VV, and HV polarization (as realized in experimental setup), where H and V represent the horizontal and vertical polarizations of the incoming and outgoing lights, as shown in Fig. 1(b). For example, in our notation HV polarization implies $\hat{\boldsymbol{\varepsilon}}_{\mathrm{in}} = H$ and $\hat{\boldsymbol{\varepsilon}}_{\mathrm{out}} = V$. The Raman signal from the isotropic TLAF can be explored by one of these three polarization choices originating from the irreducible representations $\alpha^{A_1} + \alpha^{E_1}$ (HH, VV) and α^{E_2} (HV) modes. Note, $HH = VV$ only for the anisotropic TLAF.

The noninteracting Raman spectra for the isotropic cases are shown in Fig. 4. The bimagnon spectrum is polarization independent since the red solid lines of Figs. 4(a) and 4(b) are the same. However, the trimagnon is polarization dependent since the black dashed lines of Figs. 4(a) and 4(b) behave differently. The trimagnon intensity in the HH polarization is much greater than that in the HV polarization. For the anisotropic case, the Raman signal under HH (VV) polarization and HV polarization stems from η^{A_1} and η^{A_2} mode, respectively. As the Raman scattering operator of the bimagnon in A_1 mode is commutable with H_2, the bimagnon intensity in this channel is zero [see the blue solid line in Fig. 4(a)]. Different from the two-peak feature observed in the Raman response of the isotropic TLAF in Fig. 4, the bimagnon spectrum of the anisotropic case presents a single-peak structure with a downshift in peak energy.

Previously, we discussed the importance of magnon-magnon interaction within the context of the spectral function of a TLAF. Thus, we calculated the interacting Raman multimagnon spectrum using Eq. (25). Figure 5 shows the interacting bimagnon intensity with different parameters under

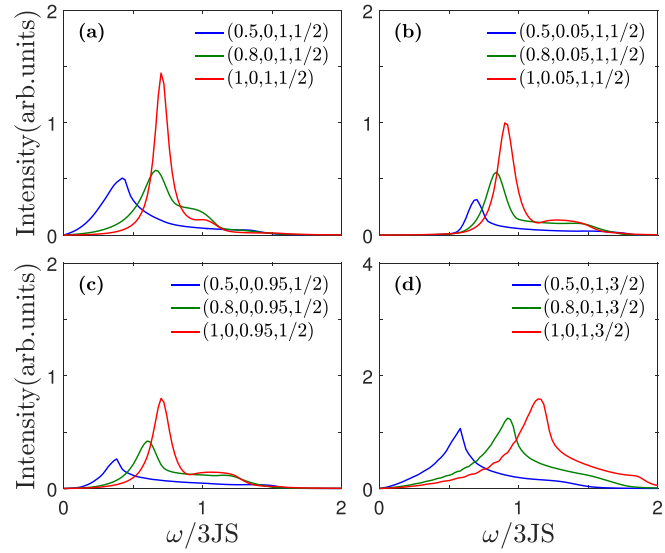

FIG. 5. Interacting Raman bimagnon spectra of spin-$\frac{1}{2}$ systems in HV polarization with different parameters (J', D, Δ, S).

HV polarization. We note that the bimagnon intensity with HH (VV) polarization is almost zero. We study the effect of magnon-magnon interactions, spatial anisotropy, DM interaction, XXZ anisotropy, and spin value on Raman bimagnon spectrum. Considering interactions, the spectrum in the HV polarization displays a single-peak structure in the isotropic model compared to the two-peak structure of the noninteracting calculation. Spatial anisotropy decreases the intensity and the peak energy. DM interaction shifts the peak towards higher energy. Although XXZ anisotropy introduces a gap, the bimagnon peak has a slight downshift in energy.

As anisotropy increases, the system tends to behave like a quasi-one-dimensional (quasi-1D) spin chain. Thus, it reduces the bimagnon intensity and leads to the downshift of the peak similar to what is predicted to occur in the RIXS spectrum [47] at the roton scattering momentum $\mathbf{q} = M$ and $\mathbf{q} = M'$. However, unlike the RIXS spectrum, the DM interaction causes a decrease in the Raman intensity [compare Fig. 5(a) to Fig. 5(b)]. The reduction effect is also seen in the XXZ model if we compare Fig. 5(a) to Fig. 5(c). This reduction can be attributed to the influence of DM interaction and XXZ anisotropy on the bimagnon scattering matrix element. With increasing spatial anisotropy, DM interaction plays a more important role. Thus, the Raman intensity reduction is more prominent in the systems with greater spatial anisotropy. The renormalized dispersion is shown in Fig. 3. DM interaction introduces a spin gap, resulting in the higher peak energy in Fig. 5(b) compared to Fig. 5(a). Although a tiny gap is generated by XXZ anisotropy, the bimagnon peak shifts to lower energy slightly in Fig. 5(c) compared to Fig. 5(a). In addition, the large spin value weakens the quantum fluctuations and magnon-magnon interactions [compare Fig. 5(d) to Fig. 5(a)]. Thus, Fig. 5(d) shows an energy upshift with vanishing shoulder, similar to the noninteracting case.

We study the Raman spectrum of two real materials $Ba_3CoSb_2O_9$ (isotropic TLAF) and Cs_2CuCl_4 (anisotropic TLAF). The Raman spectrum of $Ba_3CoSb_2O_9$ in C_{3v}

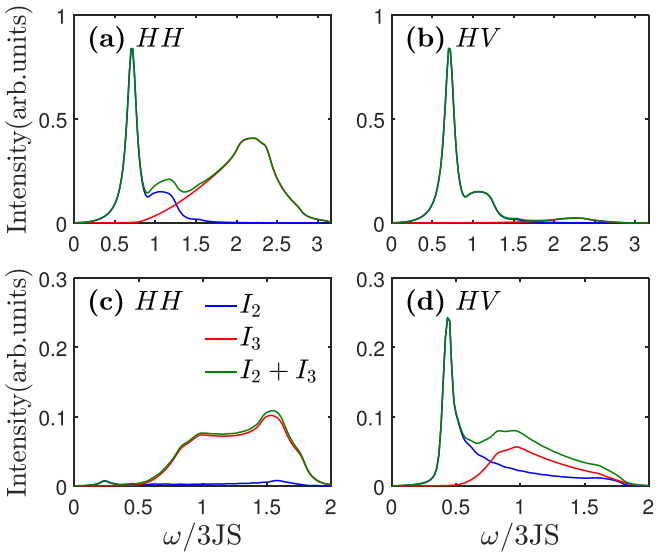

FIG. 6. Interacting bimagnon and noninteracting trimagnon Raman spectra of $Ba_3CoSb_2O_9$ and Cs_2CuCl_4. The left (right) column is under HH (HV) polarization. The first line is for $Ba_3CoSb_2O_9$ with $(J', D, \Delta) = (1, 0, 0.954)$ [50]. The second line is for Cs_2CuCl_4 with $(J', D, \Delta) = (0.316, 0.025, 1)$ [47].

symmetry is shown in Figs. 6(a) and 6(b). For $Ba_3CoSb_2O_9$, with DM interaction set to zero and $J = J'$ the ground state is close to a 120° noncollinear magnetic order. We use the parameters from the electronic spin resonance (ESR) experiment of Susuki *et al.* [50] as an input for our Raman computation. The Raman spectrum of Cs_2CuCl_4 in C_{2v} symmetry is shown in Figs. 6(c) and 6(d). The fit parameters for Cs_2CuCl_4 were chosen from our earlier TESWT INS fitting result [47].

The $Ba_3CoSb_2O_9$ Raman spectrum shows two prominent features for both the HH and HV polarizations. In the HH polarization there is a clear separation of energy excitation. The bimagnon peaks around $\approx 1.1J$, whereas the trimagnon peaks around $\approx 3.3J$. However, the bimagnon intensity is much greater than the trimagnon response in the HH polarization geometry. For the HV case, the Raman intensity is dominated by the bimagnon signal. For Cs_2CuCl_4 the bimagnon signal is almost zero in the HH channel. Thus, the trimagnon is the main contribution. This response is different from that observed in the isotropic TLAF $Ba_3CoSb_2O_9$. Hence, we can use the HH signal as a signature to identify anisotropic behavior in a TLAF. The trimagnon signal is broad and spreads over an energy range of $\approx J$–$3J$. In contrast, the HV polarization for Cs_2CuCl_4 supports a nonzero signal for both the bimagnon and the trimagnon intensities. The bimagnon peaks at $\approx 0.6J$ and the trimagnon is maximum around $\approx 1.2J$. This behavior is qualitatively similar to what we observe for $Ba_3CoSb_2O_9$ Raman signal in the HH geometry. The bimagnon intensity for $Ba_3CoSb_2O_9$ is greater than Cs_2CuCl_4. This can be explained by the presence of stronger spin coupling along the diagonal bonds for the isotropic TLAF. Furthermore, comparing Fig. 6(b) to Fig. 6(d) we find that the trimagnon response survives only in the anisotropic case, consistent with Fig. 4(b). Thus, we can also judge the degree of anisotropy of the system from the HV polarized Raman spectrum.

V. CONCLUSION

We applied TESWT to calculate the bimagnon and trimagnon Raman spectra of an isotropic and an anisotropic TLAF. We extended TESWT to the XXZ model considering both spatial anisotropy and DM interaction. Our calculation is an application of the TESWT formalism to Raman spectroscopy analysis. We computed the TESWT corrected ordering wave vector, the on-shell dispersion, the spectral function, and the Raman spectrum in both C_{3v} and C_{2v} symmetries for the HH and the HV polarizations.

Based on our calculations we find that even for our system, the spin Casimir effect can induce an arrangement of collinear spins [13]. Although DM interaction and XXZ anisotropy stabilize the spiral order, spin wave theory is unable to predict an accurate ordering wave vector for the system. Thus, one needs to account for the presence of spin Casimir torque introduced by zero-point quantum fluctuations. This reduces the range of the spiral phase. Both XXZ anisotropy and DM interaction introduce a gap at the ordering wave vector, leading to suppression of damping and magnon excitation stabilization. We note that DM interaction brings about a stronger suppression effect on magnon decay than XXZ anisotropy. We also discuss the sensitivity of Raman spectrum to polarization, system parameters (J', D, Δ, S), and magnon-magnon interactions. We find that large spin values cause an energy upshift with vanishing shoulder due to the weakened quantum fluctuations and magnon-magnon interactions. We also compute the bimagnon and trimagnon Raman spectra for $Ba_3CoSb_2O_9$ and Cs_2CuCl_4. In an isotropic TLAF, the Raman spectrum is sensitive to polarization for trimagnon excitation and independent from polarization for the bimagnon excitation. However, the converse holds true for the anisotropic lattice. The bimagnon excitation is polarization dependent. We propose that the degree of anisotropy of the system can be judged using either the HH or the HV polarization. Based on our calculations, we have shown that TESWT is a reliable method to calculate and analyze the Raman spectrum of frustrated magnetic materials. Finally, we hope that our results will inspire experimentalists to perform measurements to verify our predictions.

ACKNOWLEDGMENTS

We thank N. Drichko, R. Yu, and Z. Xiong for helpful discussions. T.D. acknowledges invitation, hospitality, and kind support from Sun Yat-Sen University. C.S., S.J., and D.X.Y. are supported by NKRDPC Grants No. 2017YFA0206203, No. 2018YFA0306001, NSFC-11974432, GBABRF-2019A1515011337, and Leading Talent Program of Guangdong Special Projects. T.D. acknowledges funding support from Sun Yat-Sen University Grants No. OEMT–2019–KF-04, No. OEMT–2017–KF–06 and Augusta University Scholarly Activity Award.

APPENDIX: (1/S)-SPIN WAVE THEORY

In this Appendix we state the expression for the functions introduced under $1/S$ LSWT, which can be easily applied under the TESWT. The classical energy $E_0(\mathbf{Q})$ is given by

$$E_0(\mathbf{Q}) = NS^2(J_{\mathbf{Q}} - \eta_{\mathbf{Q}}) = NS^2\gamma_{\mathbf{Q}}, \tag{A1}$$

with

$$J_{\mathbf{k}} = J\,\cos k_x + 2J'\cos\frac{k_x}{2}\cos\frac{\sqrt{3}}{2}k_y,$$
$$\eta_{\mathbf{k}} = 2D\,\sin\frac{k_x}{2}\cos\frac{\sqrt{3}}{2}k_y. \tag{A2}$$

The classical ordering vector Q_{cl} is obtained by solving the following self-consistent equation:

$$\nabla_{\mathbf{Q}} E_0(\mathbf{Q}) = 0. \tag{A3}$$

The bare magnon dispersion is $S\varepsilon_{\mathbf{k}}$ with

$$\varepsilon_{\mathbf{k}} = \sqrt{A_{\mathbf{k}}^2 - B_{\mathbf{k}}^2}, \tag{A4}$$

where

$$A_{\mathbf{k}} = \tfrac{1}{2}(2\Delta J_{\mathbf{k}} + \gamma_{\mathbf{Q}+\mathbf{k}} + \gamma_{\mathbf{Q}-\mathbf{k}} - 4\gamma_{\mathbf{Q}}),$$
$$B_{\mathbf{k}} = \tfrac{1}{2}(\gamma_{\mathbf{Q}+\mathbf{k}} + \gamma_{\mathbf{Q}-\mathbf{k}} - 2\Delta J_{\mathbf{k}}). \tag{A5}$$

The rest of the quadratic terms in $\mathcal{H}_{\text{eff}}$ are obtained from a mean-field decoupling of the quartic Hamiltonian with

$$\delta\varepsilon_{\mathbf{k}} = \left(u_{\mathbf{k}}^2 + v_{\mathbf{k}}^2\right)\delta A_{\mathbf{k}} + 2u_{\mathbf{k}}v_{\mathbf{k}}\delta B_{\mathbf{k}},$$
$$O_{\mathbf{k}} = \left(u_{\mathbf{k}}^2 + v_{\mathbf{k}}^2\right)\delta B_{\mathbf{k}} + 2u_{\mathbf{k}}v_{\mathbf{k}}\delta A_{\mathbf{k}}, \tag{A6}$$

where $u_{\mathbf{k}}$ and $v_{\mathbf{k}}$ are the Bogoliubov transformation coefficients given by

$$u_{\mathbf{k}} = \sqrt{\frac{A_{\mathbf{k}}}{2\varepsilon_{\mathbf{k}}} + \frac{1}{2}},$$
$$v_{\mathbf{k}} = -\text{sgn}(B_{\mathbf{k}})\sqrt{\frac{A_{\mathbf{k}}}{2\varepsilon_{\mathbf{k}}} - \frac{1}{2}}, \tag{A7}$$

and

$$\delta A_{\mathbf{k}} = \frac{A_{\mathbf{k}}}{2} + \frac{1}{2N}\sum_{\mathbf{p}}\frac{1}{\varepsilon_{\mathbf{p}}}\left[A_{\mathbf{p}}(A_{\mathbf{k}-\mathbf{p}} + B_{\mathbf{k}-\mathbf{p}} - A_{\mathbf{k}} - A_{\mathbf{p}}) + B_{\mathbf{p}}\left(\frac{B_{\mathbf{k}}}{2} + B_{\mathbf{p}}\right)\right],$$
$$\delta B_{\mathbf{k}} = \frac{B_{\mathbf{k}}}{2} - \frac{1}{2N}\sum_{\mathbf{p}}\frac{1}{\varepsilon_{\mathbf{p}}}\left[B_{\mathbf{p}}\left(A_{\mathbf{k}-\mathbf{p}} + B_{\mathbf{k}-\mathbf{p}} - \frac{A_{\mathbf{k}}}{2} - \frac{A_{\mathbf{p}}}{2}\right) + A_{\mathbf{p}}\left(B_{\mathbf{k}} + \frac{B_{\mathbf{p}}}{2}\right)\right]. \tag{A8}$$

The cubic interaction terms are defined as

$$\Phi_a(1,2;3) = [\bar{\gamma}_1(u_1 + v_1)(u_2u_3 + v_2v_3) + \bar{\gamma}_2(u_2 + v_2)(u_1u_3 + v_1v_3) - \bar{\gamma}_3(u_3 + v_3)(u_1v_2 + v_1u_2)],$$
$$\Phi_b(1,2,3) = [\bar{\gamma}_1(u_1 + v_1)(u_2v_3 + v_2u_3) + \bar{\gamma}_2(u_2 + v_2)(u_1v_3 + v_1u_3) + \bar{\gamma}_3(u_3 + v_3)(u_1v_2 + v_1u_2)], \tag{A9}$$

with

$$\bar{\gamma}_{\mathbf{k}} = \gamma_{\mathbf{Q}+\mathbf{k}} - \gamma_{\mathbf{Q}-\mathbf{k}}. \tag{A10}$$

The quartic interaction term is given by

$$\begin{aligned}\Phi_c(1,2;3,4) = &-(B_1 + B_2 + B_4)(u_1u_2u_3v_4 + v_1v_2v_3u_4) - (B_1 + B_2 + B_3)(u_1u_2v_3u_4 + v_1v_2u_3v_4)\\ &-(B_2 + B_3 + B_4)(u_1v_2u_3u_4 + v_1u_2v_3v_4) - (B_1 + B_3 + B_4)(u_1v_2v_3v_4 + v_1u_2u_3u_4)\\ &+[(C_{1-3} + C_{2-3} + C_{1-4} + C_{2-4}) - (A_1 + A_2 + A_3 + A_4)](u_1u_2u_3u_4 + v_1v_2v_3v_4)\\ &+[(C_{1+2} + C_{3+4} + C_{1-3} + C_{2-4}) - (A_1 + A_2 + A_3 + A_4)](u_1v_2u_3v_4 + v_1u_2v_3u_4)\\ &+[(C_{1+2} + C_{3+4} + C_{1-4} + C_{2-3}) - (A_1 + A_2 + A_3 + A_4)](u_1v_2v_3u_4 + v_1u_2u_3v_4),\end{aligned} \tag{A11}$$

where $C_{\mathbf{k}}$ is

$$C_{\mathbf{k}} = A_{\mathbf{k}} + B_{\mathbf{k}}. \tag{A12}$$

[1] M. Kohno, O. A. Starykh, and L. Balents, Spinons and triplons in spatially anisotropic frustrated antiferromagnets, Nat. Phys. **3**, 790 (2007).

[2] M. Swanson, J. T. Haraldsen, and R. S. Fishman, Critical anisotropies of a geometrically frustrated triangular-lattice antiferromagnet, Phys. Rev. B **79**, 184413 (2009).

[3] P. Hauke, T. Roscilde, V. Murg, J. I. Cirac, and R. Schmied, Modified spin-wave theory with ordering vector optimization: spatially anisotropic triangular lattice and $J_1 J_2 J_3$ model with heisenberg interactions, New J. Phys. **13**, 075017 (2011).

[4] A. Weichselbaum and S. R. White, Incommensurate correlations in the anisotropic triangular heisenberg lattice, Phys. Rev. B **84**, 245130 (2011).

[5] R. Chen, H. Ju, H.-C. Jiang, O. A. Starykh, and L. Balents, Ground states of spin-$\frac{1}{2}$ triangular antiferromagnets in a magnetic field, Phys. Rev. B **87**, 165123 (2013).

[6] N. Suzuki, F. Matsubara, S. Fujiki, and T. Shirakura, Absence of classical long-range order in an $s = \frac{1}{2}$ heisenberg antiferromagnet on a triangular lattice, Phys. Rev. B **90**, 184414 (2014).

[7] B. Schmidt and P. Thalmeier, Quantum fluctuations in anisotropic triangular lattices with ferromagnetic and antiferromagnetic exchange, Phys. Rev. B **89**, 184402 (2014).

[8] O. A. Starykh, W. Jin, and A. V. Chubukov, Phases of a Triangular-Lattice Antiferromagnet Near Saturation, Phys. Rev. Lett. **113**, 087204 (2014).

[9] L. Balents, Spin liquids in frustrated magnets, Nature (London) **464**, 199 (2010).

[10] U. Schollwck, J. Richter, D. J. J. Farnell, and R. F. Bishop, Quantum magnetism, Lect. Notes Phys. **645**, 135 (2004).

[11] K. Kanoda and R. Kato, Mott physics in organic conductors with triangular lattices, Annu. Rev. Condens. Matter Phys. **2**, 167 (2011).

[12] B. J. Powell and R. H. McKenzie, Quantum frustration in organic mott insulators: From spin liquids to unconventional superconductors, Rep. Prog. Phys. **74**, 056501 (2011).

[13] Z. Z. Du, H. M. Liu, Y. L. Xie, Q. H. Wang, and J.-M. Liu, Spin casimir effect in noncollinear quantum antiferromagnets: Torque equilibrium spin wave approach, Phys. Rev. B **92**, 214409 (2015).

[14] Z. Z. Du, H. M. Liu, Y. L. Xie, Q. H. Wang, and J.-M. Liu, Magnetic excitations in quasi-one-dimensional helimagnets: Magnon decays and influence of interchain interactions, Phys. Rev. B **94**, 134416 (2016).

[15] J. Ma, Y. Kamiya, T. Hong, H. B. Cao, G. Ehlers, W. Tian, C. D. Batista, Z. L. Dun, H. D. Zhou, and M. Matsuda, Static and Dynamical Properties of the Spin-1/2 Equilateral Triangular-Lattice Antiferromagnet $Ba_3CoSb_2O_9$, Phys. Rev. Lett. **116**, 087201 (2016).

[16] S. Toth, B. Lake, K. Hradil, T. Guidi, K. C. Rule, M. B. Stone, and A. T. M. N. Islam, Magnetic Soft Modes in the Distorted Triangular Antiferromagnet α-$GaCr_2O_4$, Phys. Rev. Lett. **109**, 127203 (2012).

[17] M. Songvilay, S. Petit, E. Suard, C. Martin, and F. Damay, Spin dynamics in the distorted triangular lattice antiferromagnet α-$SrCr_2O_4$, Phys. Rev. B **96**, 024416 (2017).

[18] W. Zheng, J. O. Fjærestad, R. R. P. Singh, R. H. McKenzie, and R. Coldea, Anomalous Excitation Spectra of Frustrated Quantum Antiferromagnets, Phys. Rev. Lett. **96**, 057201 (2006).

[19] W. Zheng, J. O. Fjærestad, R. R. P. Singh, R. H. McKenzie, and R. Coldea, Excitation spectra of the spin-$\frac{1}{2}$ triangular-lattice heisenberg antiferromagnet, Phys. Rev. B **74**, 224420 (2006).

[20] R. Coldea, D. A. Tennant, and Z. Tylczynski, Extended scattering continua characteristic of spin fractionalization in the two-dimensional frustrated quantum magnet Cs_2CuCl_4 observed by neutron scattering, Phys. Rev. B **68**, 134424 (2003).

[21] H. D. Zhou, C. Xu, A. M. Hallas, H. J. Silverstein, C. R. Wiebe, I. Umegaki, J. Q. Yan, T. P. Murphy, J.-H. Park, Y. Qiu, J. R. D. Copley, J. S. Gardner, and Y. Takano, Successive Phase Transitions and Extended Spin-Excitation Continuum in the s=$\frac{1}{2}$ Triangular-Lattice Antiferromagnet $Ba_3CoSb_2O_9$, Phys. Rev. Lett. **109**, 267206 (2012).

[22] J. Oh, M. D. Le, J. Jeong, J.-h. Lee, H. Woo, W.-Y. Song, T. G. Perring, W. J. L. Buyers, S.-W. Cheong, and J.-G. Park, Magnon Breakdown in a Two Dimensional Triangular Lattice Heisenberg Antiferromagnet of Multiferroic $LuMnO_3$, Phys. Rev. Lett. **111**, 257202 (2013).

[23] R. P. Feynman, *Statistical Mechanics: A Set Of Lectures (Advanced Books Classics)*, 2nd ed., Advanced Books Classics (Westview Press, Boulder, CO, 1998).

[24] S. M. Girvin, A. H. MacDonald, and P. M. Platzman, Magneto-roton theory of collective excitations in the fractional quantum hall effect, Phys. Rev. B **33**, 2481 (1986).

[25] Y. Kubo and S. Kurihara, Tunable rotons in square-lattice antiferromagnets under strong magnetic fields, Phys. Rev. B **90**, 014421 (2014).

[26] M. Powalski, G. S. Uhrig, and K. P. Schmidt, Roton Minimum as a Fingerprint of Magnon-Higgs Scattering in Ordered Quantum Antiferromagnets, Phys. Rev. Lett. **115**, 207202 (2015).

[27] O. A. Starykh, A. V. Chubukov, and A. G. Abanov, Flat spin-wave dispersion in a triangular antiferromagnet, Phys. Rev. B **74**, 180403(R) (2006).

[28] A. L. Chernyshev and M. E. Zhitomirsky, Spin waves in a triangular lattice antiferromagnet: Decays, spectrum renormalization, and singularities, Phys. Rev. B **79**, 144416 (2009).

[29] S. V. Isakov, T. Senthil, and Y. B. Kim, Ordering in Cs_2CuCl_4: Possibility of a proximate spin liquid, Phys. Rev. B **72**, 174417 (2005).

[30] J. Alicea, O. I. Motrunich, and M. P. A. Fisher, Algebraic Vortex Liquid in Spin-1/2 Triangular Antiferromagnets: Scenario for Cs_2CuCl_4, Phys. Rev. Lett. **95**, 247203 (2005).

[31] S. Yunoki and S. Sorella, Two spin liquid phases in the spatially anisotropic triangular heisenberg model, Phys. Rev. B **74**, 014408 (2006).

[32] O. A. Starykh and L. Balents, Ordering in Spatially Anisotropic Triangular Antiferromagnets, Phys. Rev. Lett. **98**, 077205 (2007).

[33] E. A. Ghioldi, A. Mezio, L. O. Manuel, R. R. P. Singh, J. Oitmaa, and A. E. Trumper, Magnons and excitation continuum in XXZ triangular antiferromagnetic model: Application to $Ba_3CoSb_2O_9$, Phys. Rev. B **91**, 134423 (2015).

[34] M. Y. Veillette, A. J. A. James, and F. H. L. Essler, Spin dynamics of the quasi-two-dimensional spin-$\frac{1}{2}$ quantum magnet Cs_2CuCl_4, Phys. Rev. B **72**, 134429 (2005).

[35] D. Dalidovich, R. Sknepnek, A. J. Berlinsky, J. Zhang, and C. Kallin, Spin structure factor of the frustrated quantum magnet Cs_2CuCl_4, Phys. Rev. B **73**, 184403 (2006).

[36] M. Mourigal, W. T. Fuhrman, A. L. Chernyshev, and M. E. Zhitomirsky, Dynamical structure factor of the triangular-lattice antiferromagnet, Phys. Rev. B **88**, 094407 (2013).

[37] K. Sugawara and I. Yamada, Raman scattering study of the triangular-lattice antiferromagnet VCl_2, J. Phys.: Condens. Matter **5**, 1427 (1993).

[38] M. Suzuki, I. Yamada, H. Kadowaki, and F. Takei, A Raman scattering investigation of the magnetic ordering in the two-dimensional triangular lattice antiferromagnet $LiCrO_2$, J. Phys.: Condens. Matter **5**, 4225 (1993).

[39] O. Aktas, K. D. Truong, T. Otani, G. Balakrishnan, M. J. Clouter, T. Kimura, and G. Quirion, Raman scattering study of delafossite magnetoelectric multiferroic compounds: $CuFeO_2$ and $CuCrO_2$, J. Phys.: Condens. Matter **24**, 036003 (2011).

[40] D. Wulferding, K.-Y. Choi, P. Lemmens, A. N. Ponomaryov, J. van Tol, A. T. M. Nazmul Islam, S. Toth, and B. Lake, Softened magnetic excitations in the s = 3/2 distorted triangular antiferromagnet α-$CaCr_2O_4$, J. Phys.: Condens. Matter **24**, 435604 (2012).

[41] M. E. Valentine, S. Koohpayeh, M. Mourigal, T. M. McQueen, C. Broholm, N. Drichko, S. E. Dutton, R. J. Cava, T. Birol, H. Das, and C. J. Fennie, Raman study of magnetic excitations and magnetoelastic coupling in α-$SrCr_2O_4$, Phys. Rev. B **91**, 144411 (2015).

[42] N. Drichko, R. Hackl, and J. A. Schlueter, Antiferromagnetic fluctuations in a quasi-two-dimensional organic superconductor detected by raman spectroscopy, Phys. Rev. B **92**, 161112(R) (2015).

[43] M. E. Valentine, T. Higo, Y. Nambu, D. Chaudhuri, J. Wen, C. Broholm, S. Nakatsuji, and N. Drichko, Impact of the Lattice on Magnetic Properties and Possible Spin Nematicity in the s = 1 Triangular Antiferromagnet $NiGa_2S_4$, Phys. Rev. Lett. **125**, 197201 (2020).

[44] F. Vernay, T. P. Devereaux, and M. J. P. Gingras, Raman scattering for triangular lattices spin-1/2 heisenberg antiferromagnets, J. Phys.: Condens. Matter **19**, 145243 (2007).

[45] N. Perkins and W. Brenig, Raman scattering in a heisenberg $s = \frac{1}{2}$ antiferromagnet on the triangular lattice, Phys. Rev. B **77**, 174412 (2008).

[46] N. B. Perkins, G.-W. Chern, and W. Brenig, Raman scattering in a heisenberg $s = \frac{1}{2}$ antiferromagnet on the anisotropic triangular lattice, Phys. Rev. B **87**, 174423 (2013).

[47] S. Jin, C. Luo, T. Datta, and D.-X. Yao, Torque Equilibrium Spin Wave Theory Study of Anisotropy and Dzyaloshinskii-Moriya Interaction Effects on the Indirect k-Edge RIXS Spectrum of a Triangular Lattice Antiferromagnet, Phys. Rev. B **100**, 054410 (2019).

[48] P. A. Fleury and R. Loudon, Scattering of light by one- and two-magnon excitations, Phys. Rev. **166**, 514 (1968).

[49] Z. Weihong, R. H. McKenzie, and R. R. P. Singh, Phase diagram for a class of spin-$\frac{1}{2}$ heisenberg models interpolating between the square-lattice, the triangular-lattice, and the linear-chain limits, Phys. Rev. B **59**, 14367 (1999).

[50] T. Susuki, N. Kurita, T. Tanaka, H. Nojiri, A. Matsuo, K. Kindo, and H. Tanaka, Magnetization Process and Collective Excitations in the s=1/2 Triangular-Lattice Heisenberg Antiferromagnet $Ba_3CoSb_2O_9$, Phys. Rev. Lett. **110**, 267201 (2013).

[51] M. Frontzek, J. T. Haraldsen, A. Podlesnyak, M. Matsuda, A. D. Christianson, R. S. Fishman, A. S. Sefat, Y. Qiu, J. R. D. Copley, S. Barilo, S. V. Shiryaev, and G. Ehlers, Magnetic excitations in the geometric frustrated multiferroic $CuCrO_2$, Phys. Rev. B **84**, 094448 (2011).

[52] S. A. Zvyagin, D. Kamenskyi, M. Ozerov, J. Wosnitza, M. Ikeda, T. Fujita, M. Hagiwara, A. I. Smirnov, T. A. Soldatov, A. Ya. Shapiro, J. Krzystek, R. Hu, H. Ryu, C. Petrovic, and M. E. Zhitomirsky, Direct Determination of Exchange Parameters in Cs_2CuBr_4 and Cs_2CuCl_4: High-Field Electron-Spin-Resonance Studies, Phys. Rev. Lett. **112**, 077206 (2014).

[53] S. A. Zvyagin, M. Ozerov, D. Kamenskyi, J. Wosnitza, J. Krzystek, D. Yoshizawa, M. Hagiwara, R. Hu, H. Ryu, C. Petrovic, and M. E. Zhitomirsky, Magnetic excitations in the spin-1/2 triangular-lattice antiferromagnet Cs_2CuBr_4, New J. Phys. **17**, 113059 (2015).

[54] J. Park, J.-G. Park, G. S. Jeon, H.-Y. Choi, C. Lee, W. Jo, R. Bewley, K. A. McEwen, and T. G. Perring, Magnetic ordering and spin-liquid state of $YMnO_3$, Phys. Rev. B **68**, 104426 (2003).

[55] Y. Shirata, H. Tanaka, A. Matsuo, and K. Kindo, Experimental Realization of a Spin-1/2 Triangular-Lattice Heisenberg Antiferromagnet, Phys. Rev. Lett. **108**, 057205 (2012).

[56] G. Koutroulakis, T. Zhou, Y. Kamiya, J. D. Thompson, H. D. Zhou, C. D. Batista, and S. E. Brown, Quantum phase diagram of the $s = \frac{1}{2}$ triangular-lattice antiferromagnet $Ba_3CoSb_2O_9$, Phys. Rev. B **91**, 024410 (2015).

[57] D. Yamamoto, G. Marmorini, and I. Danshita, Quantum Phase Diagram of the Triangular-Lattice xxz Model in a Magnetic Field, Phys. Rev. Lett. **112**, 127203 (2014).

[58] D. Yamamoto, G. Marmorini, and I. Danshita, Erratum: Quantum Phase Diagram of the Triangular-Lattice xxz Model in a Magnetic Field, Phys. Rev. Lett. **112**, 259901 (2014).

[59] D. Yamamoto, G. Marmorini, and I. Danshita, Microscopic Model Calculations for the Magnetization Process of Layered Triangular-Lattice Quantum Antiferromagnets, Phys. Rev. Lett. **114**, 027201 (2015).

[60] C. Liu, A. Zhang, Q. Zhang, R. Yu, and X. Wang, Spin-wave approach to the two-magnon raman scattering in a J_{1x}–J_{1y}–J_2–J_c antiferromagnetic Heisenberg model, Phys. Rev. B **95**, 104431 (2017).

[61] W. Heitler, *The Quantum Theory of Radiation* (Dover, New York, 1954).

[62] R. Loudon, The Raman effect in crystals, Adv. Phys. **13**, 423 (1964).

[63] T. Moriya, Theory of light scattering by magnetic crystals, J. Phys. Soc. Jpn. **23**, 490 (1967).

[64] C. Luo, T. Datta, Z. Huang, and D.-X. Yao, Signatures of indirect k-edge resonant inelastic x-ray scattering on magnetic excitations in a triangular-lattice antiferromagnet, Phys. Rev. B **92**, 035109 (2015).